Remote Sensing of Environment 251 (2020) 112114

Contents lists available at ScienceDirect

Remote Sensing of Environment

journal homepage: www.elsevier.com/locate/rse

Estimating wildfire fuel consumption with multitemporal airborne laser scanning data and demonstrating linkage with MODIS-derived fire radiative energy

T. Ryan McCarley[a,*], Andrew T. Hudak[b], Aaron M. Sparks[a], Nicole M. Vaillant[c], Arjan J.H. Meddens[d], Laura Trader[e], Francisco Mauro[f], Jason Kreitler[g], Luigi Boschetti[a]

[a] University of Idaho, College of Natural Resources, Moscow, ID 83844, USA
[b] U.S. Department of Agriculture Forest Service, Rocky Mountain Research Station, Moscow, ID 83843, USA
[c] U.S. Department of Agriculture Forest Service, Rocky Mountain Research Station, Wildland Fire Management, Research, Development and Applications, Bend, OR 97701, USA
[d] Washington State University, School of the Environment, Pullman, WA 99164, USA
[e] National Parks Service, Bandelier National Monument, Los Alamos, NM 87544, USA
[f] Oregon State University, College of Forestry, Corvallis, OR 97331, USA
[g] U.S. Geological Survey, Western Geographic Science Center, Boise, ID 83706, USA

ARTICLE INFO

Keywords:
Airborne lidar
Fire
Forest biomass
Carbon emissions
Eastern cascade range
Bandelier national monument

ABSTRACT

Characterizing pre- and post-fire fuels remains a key challenge for estimating biomass consumption and carbon emissions from wildfires. Airborne laser scanning (ALS) data have demonstrated effectiveness for estimating canopy, and to a lesser degree, surface fuel components at fine-scale (i.e., 30 m) across landscapes. Using pre- and post-fire ALS data and corresponding field data, this study estimated consumption of canopy fuel (ΔCF), understory fuel (ΔUF), total fuel (ΔTF), and canopy bulk density (ΔCBD) for the 2012 Pole Creek fire in Oregon, USA (10,760 ha), and portions of the 2011 Las Conchas fire in New Mexico, USA (4,934 ha). Additionally, the feasibility of predicting fuel consumption was tested using separate pre- and post-fire models (PrePost), models combining all pre- and post-fire data (Pooled), and models using all data from both fires (Global). Estimates of ΔTF were then compared to fire radiative energy (FRE, units: MJ) derived from Fire Radiative Power (FRP, units: MW) observations from the Moderate Resolution Imaging Spectroradiometer (MODIS) sensor onboard NASA Terra and Aqua satellites to mechanistically derive a biomass combustion coefficient (BCC, units: kg MJ^{-1}). The PrePost and Pooled approaches yielded similar results at Las Conchas, but at Pole Creek insufficient pre-fire field data resulted in erroneous fuel consumption estimates outside the fire perimeter using the PrePost models. These results demonstrated that pre-fire field data were less important for these models than having field data which represent the full range of fuel conditions likely to exist across the landscape. Estimated total biomass consumed for the PrePost, Pooled, and Global models were 226 Gg, 224 Gg, and 224 Gg at Las Conchas, and 581 Gg, 713 Gg, and 552 Gg at Pole Creek. Comparisons between estimated ΔTF and FRE yielded an average BCC for both fires of 0.367 (s.d. ± 0.049) kg MJ^{-1} based on pixels with at least five MODIS observations. Both higher MODIS observations per pixel and accounting for canopy occlusion of FRE improved the relationship between ΔTF and MODIS-FRE. This study suggested a practical modelling approach for future efforts using only post-fire field observations and quantified a landscape-scale relationship between MODIS-derived FRE and fine-scale fuel consumption consistent with prior experiments.

1. Introduction

Wildfire is a significant contributor to the global carbon cycle (Bowman et al., 2009) and is intricately linked with climate change through anthropogenic forcing and positive feedback (Abatzoglou and Williams, 2016; Westerling et al., 2006). Globally, fires are estimated to emit between 1.8 and 3.9 Pg C yr^{-1} (Andreae and Merlet, 2001; Van Der Werf et al., 2017; Van Der Werf et al., 2010; Van Der Werf et al., 2004). These global carbon estimates are conventionally derived from a bottom-up approach using the equation presented by Seiler and Crutzen (1980):

* Corresponding author.
E-mail address: tmccarley@uidaho.edu (T.R. McCarley).

https://doi.org/10.1016/j.rse.2020.112114
Received 8 May 2020; Received in revised form 2 September 2020; Accepted 24 September 2020
0034-4257/ © 2020 Elsevier Inc. All rights reserved.

$$M = A\beta\rho \quad (1)$$

where M is biomass consumption (Mg), A is the area burned (ha), β is the biomass of pre-fire fuel load (Mg ha^{-1}), and ρ is the combustion completeness (%). Biomass consumption (M) is then multiplied by an emission factor, usually 0.45 to 0.5, to estimate the proportion of carbon (French et al., 2011). Therefore, uncertainty in global carbon estimates stems from the difficulty in accurately quantifying each of the parameters in Eq. (1) (Smith et al., 2005; Wooster et al., 2005) as well as the emission factor (Andreae and Merlet, 2001).

The term fuel can be used to describe multiple properties of vegetative matter available for combustion, such as chemistry, quantity, density, geometry, and continuity (Ottmar, 2014), but in Eq. (1), fuel load describes the quantity (i.e., biomass) of all combustible material. Fuel load remains one of the most difficult variables to quantify regionally and globally due to the high spatial variability of biomass across landscapes (Chuvieco et al., 2019; García et al., 2017) and the difficulty for optical satellite sensors to estimate the portion of fuel load occluded by forest canopies (Falkowski et al., 2005; Riaño et al., 2002). Advances in remote sensing, in particular the development of global, multiyear burned area products (Giglio et al., 2018; Van Der Werf et al., 2017) and detection of small fires (Randerson et al., 2012; Roteta et al., 2019), have significantly reduced the uncertainty in burned area estimates (Chuvieco et al., 2019). Other recent efforts have sought to use Landsat and Sentinel satellites to estimate the product of the burned sub-pixel fraction and combustion completeness, known as *f.cc* (Roy et al., 2019; Roy and Landmann, 2005). Research is underway to resolve emissions factors at multiple scales, but these too require accurate quantification of fuel load (Prichard et al., 2019).

An alternative approach for estimating biomass consumption is to measure the energy released by combustion from Earth observing sensors such as the Moderate Resolution Imaging Spectroradiometer (MODIS) sensor onboard NASA Terra and Aqua satellites, the underlying assumption being that the energy released is proportionate to the biomass consumed (Kaufman et al., 1996). The instantaneous radiative component of the fire reaction, fire radiative power (FRP; units: W), has been shown to be linearly related to the rate of biomass consumption (Freeborn et al., 2011; Wooster, 2002; Wooster et al., 2005), while integrating FRP measurements over time allows for the estimation of Fire Radiative Energy (FRE; units: J). FRE has been demonstrated to be linearly related to the total biomass consumption, yielding a biomass combustion coefficient (BCC), at multiple scales including: laboratory experiments (Freeborn et al., 2008; Smith et al., 2013; Wooster et al., 2005), small-scale outdoor experiments (Kremens et al., 2012), forest stand-scale fires (Hudak et al., 2016b; Klauberg et al., 2018), and fires at regional scales, such as the conterminous U.S. (Li et al., 2018). Li et al. (2018) derived a BCC of 0.301 kg MJ^{-1} comparing MODIS radiative energy measurements with biomass consumption derived from the Landscape Fire and Resource Planning Tools (LANDFIRE; www.landfire.gov) Fuel Characteristic Classification System fuel bed types (FCCS; Ottmar et al., 2007) and burned area from the Monitoring Trends in Burn Severity project (MTBS; Eidenshink et al., 2007). However, there is uncertainty in this approach due to MTBS burned area commission errors (Sparks et al., 2015), subjectivity of burn severity thresholds used by MTBS (Kolden et al., 2015), and the broad scope of LANDFIRE FCCS, which may not reflect short-term fuel load changes (Li et al., 2018) or local variability (McKenzie et al., 2007). Therefore, mechanistic linkage between MODIS radiative energy measurements and biomass consumption at the landscape-scale (i.e., the scale at which individual wildfires might occur) is still needed to further parameterize the BCC derived from laboratory and small outdoor experiments.

Airborne laser scanning data (ALS) data have been used to estimate fuel load (Andersen et al., 2005; Bright et al., 2017) and density (Andersen et al., 2005; Riaño et al., 2004; Riaño et al., 2003), suggesting that ALS data from before and after a fire could be used to estimate fuel consumption. ALS data capture forest structure by actively measuring the distances from the sensor to trees and other objects on the ground with active laser pulses. These individual observations, each with an x, y location, and z height, are assembled into a point cloud resembling the structure of vegetation. Multiple height and density statistics representing structure are then used to model biophysical variables like biomass. Fuel load can compose all burnable biomass, but often fuels are grouped into components such as canopy, shrubs, nonwoody vegetation, down woody debris, litter, and duff (Ottmar, 2014). Thus, using multiple different metrics of forest structure, the biomass of individual fuel load components can also be modelled.

As the number of ALS data collections increases, more studies have incorporated multitemporal ALS data (i.e., the use of two or more ALS datasets across time at a given location). Some studies have explored the correlation between multitemporal ALS data and multitemporal multispectral data for quantifying structural changes brought about by wildfire (McCarley et al., 2018; McCarley et al., 2017; Wulder et al., 2009); however, a recent wave of research has demonstrated that multitemporal ALS data observations by themselves are effective for measuring biophysical fire effects such as basal area mortality (Hoe et al., 2018; Hu et al., 2019), reduction in leaf area index (Hu et al., 2019), decrease in canopy volume (Alonzo et al., 2017), and depth of boreal peat loss (Chasmer et al., 2017). Multitemporal ALS data have also been effective at quantifying fuel load and density changes from forest harvest (Fekety et al., 2015; Hudak et al., 2012), fuel treatments (Ma et al., 2018), insect defoliation (Meng et al., 2018; Skowronski et al., 2014), wind storms (Zhao et al., 2018), and forest growth (Fekety et al., 2015; Hudak et al., 2012; Skowronski et al., 2014; Zhao et al., 2018).

Estimating fuel load or density from ALS data requires models trained from field observations, which are not always available for an unpredictable disturbance such as wildfire. In cases where there are field observations, they may be only pre-fire, or more often only post-fire data, but rarely are both available (Alonzo et al., 2017; Hoe et al., 2018). This limitation places a high priority on research to evaluate model generality and transferability (i.e., the ability for a model to accurately predict values across space and time). Other studies have demonstrated that fuel load models developed from field data and ALS data at a single point in time could be used to make predictions with ALS data in similar ecosystems (Fekety et al., 2018) and that predictions fit for one year could be applied to other years (Fekety et al., 2015; Zhao et al., 2018). However, generality and transferability of ALS fuel models have not been tested for quantifying fuel consumption in a wildfire.

The principal goals and objectives of this study were to produce fuel consumption estimates at a fine-scale (i.e., 30 m) for two fires in western U.S. forested ecosystems using multitemporal ALS and field data, thereby offering a novel solution for parameterizing the landscape-scale relationship between MODIS-derived FRE and fine-scale fuel consumption. The measures of fuel load consumption predicted in this study were change in canopy fuel (ΔCF), understory fuel (ΔUF; including shrubs, nonwoody vegetation, down woody debris, litter, and duff), and total fuel (ΔTF; both canopy and understory fuel). Change in canopy bulk density (ΔCBD), a measure of fuel density consumption, was also predicted. To achieve the best model performance, the feasibility of predicting fuels over time (i.e., temporal generalization) and between fires (i.e., spatial generalization) was tested. Finally, a biomass combustion coefficient (BCC) between MODIS-derived FRE and ΔTF was developed and compared to prior studies, with additional attention to the effects of canopy occlusion and the number of MODIS observations.

2. Material and methods

2.1. Study area

This study used multitemporal ALS and field data from the 2011 Las Conchas fire (61,057 ha) in northern New Mexico, USA and the 2012 Pole Creek fire (10,760 ha) in the eastern Cascade Range of central

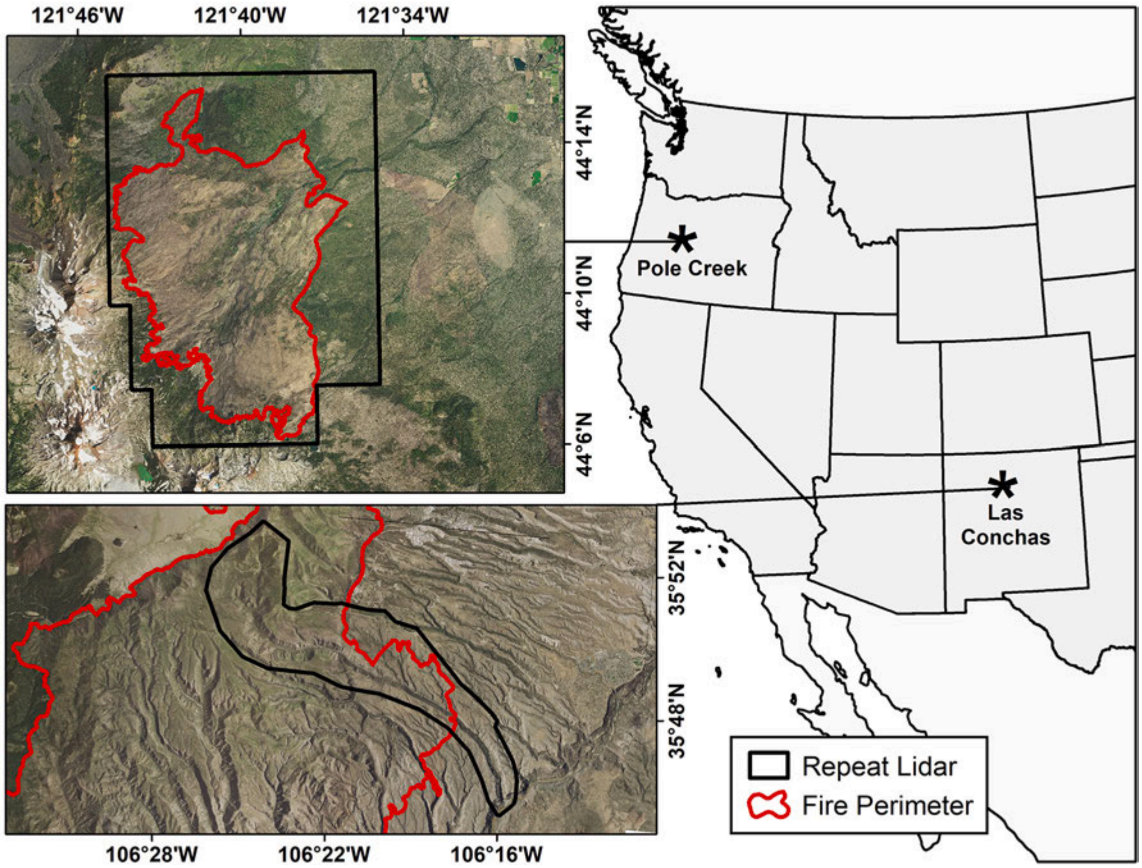

Fig. 1. Location of the Pole Creek (Oregon, USA) and Las Conchas (New Mexico, USA) fires, with fire perimeter and footprint for the overlapping airborne laser scanning (ALS) data surveys overlaid on 2014 National Agricultural Imagery Program (NAIP) imagery.

Oregon, USA (Fig. 1). Both fires experienced a wide range of fire behavior, from high-intensity crown fire to low-intensity surface fire. The Las Conchas fire area is characterized by a steep gradient in precipitation as a function of elevation which ranges from 1,600 to 2,900 m. This gradient results in vegetation ranging from mixed conifer forest at the highest elevations, to ponderosa pine in the canyons and mesa-tops, to pinyon-juniper woodlands at the lowest elevations. The most common tree species observed in field sites were ponderosa pine (*Pinus ponderosa*), white fir (*Abies concolor*), Douglas-fir (*Pseudotsuga menziesii*), quaking aspen (*Populus tremuloides*), and gambel oak (*Quercus gambelii*). Repeat ALS data were available for 6,997 ha of the Frijoles watershed, 4,934 ha of which were burned by the Las Conchas fire. Average forest canopy cover (i.e., percent of first returns above 2 m) before the fire was 32% (s.d. ± 27%).

The entire Pole Creek fire extent and adjacent forest, totaling 22,210 ha, were captured by repeat ALS data acquisitions. Elevation at Pole Creek starts at 1,200 m, where relatively flat, open ponderosa pine woodlands are dominant. The elevation gradually increases to 2,100 m, with forest composition changing from mixed conifer and lodgepole pine to mountain hemlock at the highest elevations. The area can be further characterized by its proximity to active volcanoes, which influence weather, topography, and soils. The most common tree species observed in field sites were ponderosa pine, lodgepole pine (*Pinus contorta*), mountain hemlock (*Tsuga mertensiana*), and grand fir (*Abies grandis*). Average forest canopy cover before the fire was 44% (s.d. ± 22%).

2.2. Data acquisition and pre-processing

2.2.1. Field plot data

Field data for the Las Conchas fire were collected by the National Park Service in permanent 20 m by 50 m fixed plots (see Appendix A for plot design). A total of 57 pre-fire field plots were measured in either 2008, 2009, or 2010 while 78 post-fire field plots were measured in 2012, 2015, or 2016. For the post-fire plots, 48 were repeat measurements of existing pre-fire plots, and 12 were located outside the fire perimeter. For the Pole Creek fire, 9 pre-fire field plots were measured by the FIA program (Gillespie, 1999) in 2007, 2009, 2010, 2011, or 2012. A total of 72 post-fire plots were measured in 2013 by the USDA Forest Service Western Wildland Environmental Threat Assessment Center and the University of Idaho. All post-fire plots were inside the fire perimeter, and none were repeat measurements (see Appendix A for plot design).

Pre- and post-fire field data suitable for calculating FCCS strata described in Ottmar (2014) were available for both fires. Individual fuel load components were grouped into canopy fuels (CF; trees, snags, ladder fuel) and understory fuels (UF; shrubs, nonwoody vegetation, woody fuels, litter, and duff). Using the Fire and Fuels Extension to the Forest Vegetation Simulator (FFE-FVS; Reinhardt and Crookston, 2003), CF was derived from the sum of all live trees, snags, and tree crowns (see Appendix A for more detail). CBD was also obtained from the FFE-FVS Potential Fire table, following methods described in Scott and Reinhardt (2001). For all field plots at Las Conchas, and post-fire field plots at Pole Creek, UF was calculated using equations from Brown et al. (1982). UF estimates for the pre-fire field plots at Pole Creek were already included in the aggregated plot data received from FIA. Early analysis indicated that litter and duff values were more reliable using the aggregated plot data rather than at the FIA subplot level, and that spatial autocorrelation was limited. Therefore, aggregated plot data (n = 9) were used rather than treating each individual subplot (n = 36) as a data point. Summary pre- and post-fire plot statistics for each variable are reported in Table 1.

Table 1
Summary statistics for field plot data at the Las Conchas, New Mexico (LC), and Pole Creek, Oregon (PC), fires.

	Min	25th pct.	50th pct.	75th pct.	Max	Mean	Count
Canopy Fuel (Mg ha^{-1})							
LC Pre-fire	0.5	12.2	63.8	131.0	280.1	77.2	57
LC Post-fire	0.4	19.9	67.3	99.0	214.5	69.3	78
PC Pre-fire	47.6	63.9	198.0	270.1	374.1	178.9	9
PC Post-fire	1.4	33.8	100.9	194.1	511.5	126.2	72
Understory Fuel (Mg ha^{-1})							
LC Pre-fire	4.9	16.2	39.9	77.0	165.2	51.3	57
LC Post-fire	5.1	17.3	28.4	45.5	113.8	35.0	78
PC Pre-fire	24.9	32.1	50.6	74.7	124.3	57.6	9
PC Post-fire	0.1	5.9	10.7	24.3	128.8	18.5	72
Total Fuel (Mg ha^{-1})							
LC Pre-fire	7.2	27.9	107.2	208.3	382.7	128.5	57
LC Post-fire	5.5	65.6	109.7	137.0	274.9	104.3	78
PC Pre-fire	81.4	88.7	264.4	350.4	498.4	236.5	9
PC Post-fire	5.1	43.8	120.9	213.4	528.1	144.7	72
Canopy Bulk Density (kg m^{-3})							
LC Pre-fire	0.00	0.02	0.09	0.16	0.35	0.10	57
LC Post-fire	0.00	0.00	0.03	0.08	0.21	0.05	78
PC Pre-fire	0.03	0.06	0.10	0.13	0.18	0.10	9
PC Post-fire	0.00	0.00	0.03	0.07	0.29	0.05	72

2.2.2. ALS data

ALS data (Table 2) were acquired and pre-processed by The National Center for Airborne Laser Mapping (pre-fire) and Atlantic (post-fire) at Las Conchas and by Watershed Science, Inc., at Pole Creek. Pre-processing included checking vertical accuracy against monumented control points and classifying ALS returns using the proprietary software TerraScan. For this study, classified ground returns were used to generate DEMs and height normalize the ALS point clouds in the software program LAStools (Isenburg, 2013). During the LAStools height normalization process, outliers below −30 m and above 150 m were removed from the point clouds following a standard U.S. Forest Service procedure (*pers. comm.,* R. McGaughey, USFS). Pre- and post-fire DEMs were compared to validate vertical accuracy between time steps. The percent of pre- and post-fire DEM pixels (at 1 m spatial resolution) within 0.15 m vertically was 70% at Las Conchas and 81.3% at Pole Creek. For both fires, over 96% of pixels were within 0.5 m vertically. At Las Conchas, both the pre- and post-fire ALS data were delivered in the same spatial projection, but at Pole Creek, the pre-fire ALS data were re-projected in LAStools to match the post-fire projection.

Following re-projection and height normalization, the ALS point cloud data were gridded into 30 m rasters in LAStools by computing height and density metrics of the point cloud within each raster cell (Table 3). Candidate ALS metrics were based on standard outputs from FUSION software (McGaughey, 2014) and height cutoffs recommended by the U.S. Forest Service (*pers. comm.,* R. McGaughey, USFS). Similar

Table 2
Characteristics of pre- and post-fire airborne laser scanning (ALS) data acquisitions.

	Las conchas fire (Jun 2011)		Pole creek fire (Sep 2012)	
Year	2010	2013	2009	2013
Date(s) of acquisition	29-Jun to 8-Jul	24-Sep to 28-Sep	7-Oct to 11-Oct	8-Oct to 11-Oct
ALS System	Gemini 06SEN/ CON195	Leica ALS70-HP	Leica ALS50	Leica ALS50
Wavelength	1064 nm	1064 nm	1064 nm	1064 nm
Flight Altitude	600 m	1400 m	900 m	900 m
Swath Overlap	50%	50%	50%	50%
Point Density	10.28 p/m^2	8 p/m^2	8 p/m^2	8 p/m^2
Scan Frequency	60 Hz	59.8 Hz	52 Hz	52 Hz
Scan Angle	28°	30°	28°	28°

Table 3
Airborne laser scanning (ALS) metrics of forest structure. Additional metrics were considered, but not selected because they were highly correlated or multi-collinear with other variables or had low importance in the random forest (RF) models.

ALS metric	Statistic of the ALS point cloud
PCT 0-0.5 m	Percent of all returns ≤0.5 m
PCT 0.5-1 m	Percent of all returns > 0.5 m and ≤1 m
PCT 1-2 m	Percent of all returns > 1 m and ≤2 m
PCT 2-4 m	Percent of all returns > 2 m and ≤4 m
PCT 4-8 m	Percent of all returns > 4 m and ≤8 m
PCT 8-16 m	Percent of all returns > 8 m and ≤16 m
PCT 16-32 m	Percent of all returns > 16 m and ≤32 m
PCT 32-48 m	Percent of all returns > 32 m and ≤48 m
PCT 0.5-1 m (lt2)	Percent of returns (< 2 m only) > 0.5 m and ≤1 m
PCT 1-2 m (lt2)	Percent of returns (< 2 m only) > 1 m and ≤2 m
AVG	Average height of all returns
COV	Percent of first returns ≥2 m
P25	25th percentile of the height values for all returns
P50	50th percentile of the height values for all returns
P75	75th percentile of the height values for all returns
P90	90th percentile of the height values for all returns
P95	95th percentile of the height values for all returns
P01 (gt2)	1st percentile of the height values for returns ≥2 m
P05 (gt2)	5th percentile of the height values for returns ≥2 m
P10 (gt2)	10th percentile of the height values for returns ≥2 m
P25 (gt2)	25th percentile of the height values for returns ≥2 m
P50 (gt2)	50th percentile of the height values for returns ≥2 m
STD (gt2)	Skewness of the height values for returns ≥2 m
P50 (lt2)	50th percentile of the height values for returns < 2 m
P75 (lt2)	75th percentile of the height values for returns < 2 m
P90 (lt2)	90th percentile of the height values for returns < 2 m
P95 (lt2)	95th percentile of the height values for returns < 2 m
P99 (lt2)	99th percentile of the height values for returns < 2 m
STD (lt2)	Standard deviation of the height values for returns < 2 m

ALS height and density metrics have been used for fuel modelling in the western U.S. (Bright et al., 2017; Fekety et al., 2015; Hudak et al., 2012), Australia (Price and Gordon, 2016), and Europe (González-Ferreiro et al., 2014), provided local field data were used to train the fuel models. ALS point cloud data were clipped to field plot locations using the R package ‘lidR’ (Roussel and Auty, 2019), with measurement dates corresponding to either pre- or post-fire. Metrics were calculated from the plot-scale point clouds using the same parameters in LAStools as the grid metrics. The plot-scale metrics were used for model training and the grid metrics were used to apply the models across the landscape.

2.2.3. MODIS active fire product and fire radiative energy estimation

The Level 2 MODIS active fire product, with nominal 1 km spatial resolution, detects and characterizes FRP from fires that are observed at the time of Terra (MOD14) and Aqua (MYD14) satellite overpass (Giglio et al., 2016). Depending on cloud cover, up to four observations per day could be collected at the latitude of the study fires. For the Collection 6 MODIS active fire product (Giglio et al., 2016), FRP is calculated from the radiance sensed in the mid-infrared wavelength (3.9 μm) channel as:

$$FRP\ [MW] = \frac{A_{pix}\sigma}{aT_{MIR}}(L_{MIR} - L_{BMIR}) \tag{2}$$

where L_{MIR} is the mid-infrared radiance of fire pixels, L_{BMIR} is the radiance of neighboring non-fire background pixels, A_{pix} is the area of the MODIS pixels, σ is the Stefan-Boltzmann constant (5.6704 × 10^{-8} Wm^{-2} K^{-4}), a is a sensor-specific constant (3.0 × 10^{-9} Wm^{-2} sr^{-1} μm^{-1}), and T_{MIR} is atmospheric transmittance for the mid-infrared channel.

Estimated FRP and the associated confidence level were provided by the MOD14/MYD14 products for each detected fire pixel. All confidence levels were used for maximum fire detectability. To estimate

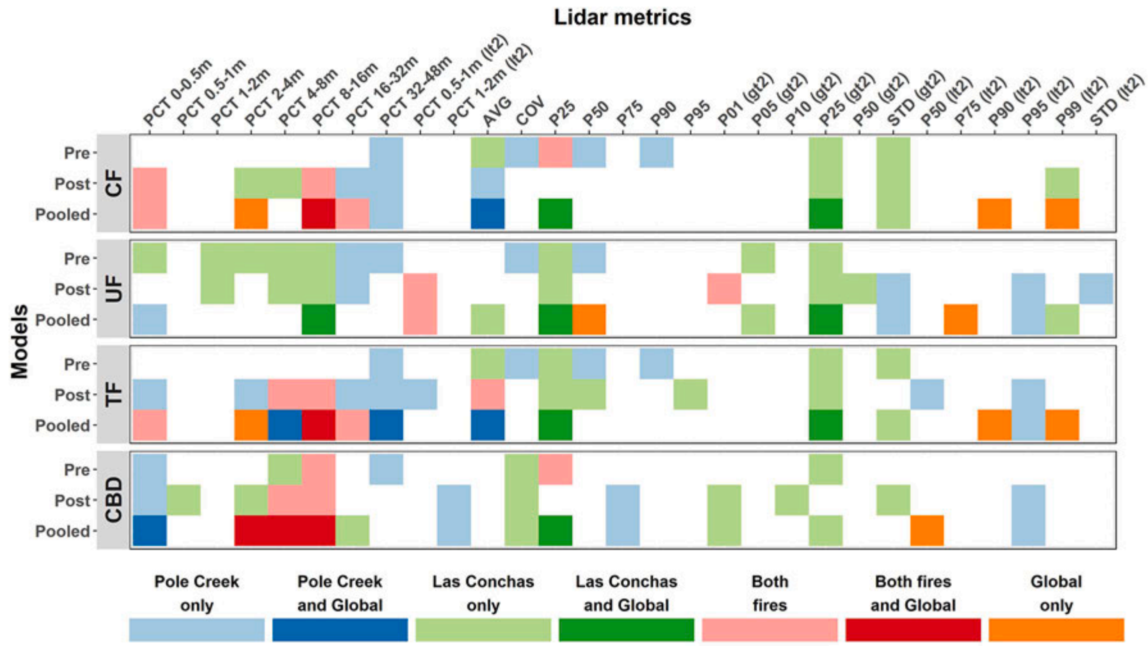

Fig. 2. Airborne laser scanning (ALS) metric selection results for modelling canopy fuel (CF), understory fuel (UF: includes shrubs, nonwoody vegetation, down woody debris, litter, and duff), total fuel (TF), and canopy bulk density (CBD). Metrics acronyms are further described in Table 3. Matrix colors denote which metrics were selected for each model and which field data were used. 'Both fires' indicates that the metric was selected by both single-fire models, whereas the 'Global' model used all data from both fires.

fire radiative energy, the MOD14 and MYD14 data were first re-projected to 1 km MODIS sinusoidal equal area using nearest neighbor resampling, following Boschetti and Roy (2009). This method mitigated the effect of increasing pixel size at higher MODIS scan angles, preventing the introduction of bias in the resampled FRP. FRE is derived through the equation:

$$FRE\ [MJ] = \sum_{i=1}^{n_i} FRP_i \Delta t_i \tag{3}$$

where n_i is the number of observations and Δt_i is the time between observations. FRE was calculated for each MODIS pixel following Boschetti and Roy (2009), assuming that FRP varied linearly between observations.

2.3. Analysis

2.3.1. Estimating fuel consumption

In this study, temporal generalization refers to the ability of a model built using data from multiple points in time (i.e., pre- and post-fire) to accurately predict fuel load and density regardless of the time period the model is applied to. Two approaches were employed to assess temporal generalization of the fuel models. The non-generalized approach, hereafter termed the PrePost model, used pre-fire ALS data and field observations to model pre-fire fuels (Pre model) and post-fire ALS data and field observations to model the post-fire fuels (Post model) separately. The Pre and Post models were then applied to the gridded ALS metrics of the corresponding time (i.e., pre- or post-fire) to map the fuels. The resulting pre- and post-fire fuel estimates (as 30 m rasters) were then differenced to obtain fuel consumption. The temporally generalized approach, hereafter termed the Pooled model, used pre- and post-fire ALS data matched with pre- and post-fire field observations to train a single combined model. The Pooled model was then applied to the pre- and post-fire gridded ALS metrics to map fuels, and the results were differenced to obtain a measure of change.

Much like the pooled approach for temporal generalization, spatial generalization refers to the ability of a model built using data from multiple regions (i.e., the two fires in this study) to accurately predict fuel load and density across regions. A spatially generalized model, hereafter termed the Global model, used pre- and post-fire ALS data matched with pre- and post-fire field observations for both fires to train a single combined model. This model was then applied to the pre- and post-fire gridded ALS metrics to map the fuel attributes at both fires. Results were differenced at each fire to obtain fuel consumption.

The models derived from the PrePost, Pooled, and Global approaches were compared using measures of model fit (r-squared, Root Mean Squared Error (RMSE), and RMSE relative to the range of observed values (RMSE%)) and direction of bias (Mean Bias Error (MBE) based on predicted minus observed values). The landscape-scale predictions of fuel consumption were assessed visually to see if they matched known disturbances, such as fire and forest harvest. Finally, predicted fuel consumption estimates were evaluated outside the fire perimeters by testing if the average consumption values were near zero in relatively unchanged areas. Because forest management activities were known to have occurred between the ALS collections at Pole Creek, the US Forest Service Forest Activity Tracking System (FACTS; USDA Forest Service, 2015) was used as a reference for timber harvest and hazard fuel reduction activities. For each model, areas where these activities occurred between ALS acquisitions were omitted when testing if average unburned predictions were near zero.

For all models the Random Forest (RF) algorithm (Breiman, 2001) was used for the following reasons: It captures potential non-linear relations, it's non-parametric nature allows prediction of multiple responses without making assumptions on the distribution of those responses, it generates variable importance, and it has demonstrated effectiveness in the estimation of fuel load (Fekety et al., 2015; Hudak et al., 2012) and fuel density (Bright et al., 2017) from ALS data. Pre-fire, post-fire, and pooled models for each variable were run separately, but with an identical procedure. ALS metrics for each model (Fig. 2) were selected using a custom model selection function that incorporated the Model Improvement Ratio (MIR; Murphy et al., 2010) and 'rfUtilities' R library (Evans and Murphy, 2017). The candidate metrics were first revised so that variables with lower importance among highly correlated variables (Pearson's $r > 0.9$) were removed from consideration, as were multi-collinear variables using a Gram-

Table 4
Model performance at both fires using pre-fire field data (Pre), post-fire field data (Post), both pre- and post-fire field data (Pooled), and both pre- and post-fire data from both fires (Global). Plots comparing field observations and model predictions are displayed in Appendix A, Fig. S1 for Las Conchas and Fig. S2 for Pole Creek.

	Model performance				Model performance			
	Las Conchas Fire				Pole Creek Fire			
	r-squared	RMSE	RMSE	MBE	r-squared	RMSE	RMSE	MBE
Canopy Fuel		Mg ha^{-1}	%	Mg ha^{-1}		Mg ha^{-1}	%	Mg ha^{-1}
Pre	0.84	26.12	9.34	−0.24	0.61	79.70	24.41	−10.83
Post	0.72	27.37	12.78	1.17	0.71	60.11	11.78	−3.55
Pooled	0.80	26.03	9.31	−0.60	0.71	60.09	11.78	−2.67
Global	0.64	52.63	10.30	−0.003	0.64	52.63	10.30	−0.003
Understory Fuel		Mg ha^{-1}	%	Mg ha^{-1}		Mg ha^{-1}	%	Mg ha^{-1}
Pre	0.63	24.38	15.21	0.83	0.50	21.86	21.99	−3.72
Post	0.16	23.26	21.40	0.71	0.20	18.31	14.23	0.31
Pooled	0.43	24.94	15.56	0.09	0.34	20.22	15.71	0.12
Global	0.42	24.07	14.58	0.42	0.42	24.07	14.58	0.42
Total Fuel		Mg ha^{-1}	%	Mg ha^{-1}		Mg ha^{-1}	%	Mg ha^{-1}
Pre	0.83	41.82	11.14	−0.57	0.57	103.87	24.91	−19.77
Post	0.64	37.05	13.75	0.89	0.73	59.53	11.38	−1.02
Pooled	0.74	41.62	11.03	−0.39	0.74	61.74	11.80	−1.67
Global	0.68	56.76	10.85	−0.03	0.68	56.76	10.85	−0.03
Canopy Bulk Density		kg m^{3}	%	kg m^{3}		kg m^{3}	%	kg m^{3}
Pre	0.71	0.04	12.75	−0.0004	0.22	0.04	29.52	−0.003
Post	0.56	0.03	15.99	0.0004	0.60	0.04	12.76	−0.001
Pooled	0.66	0.04	11.73	−0.001	0.68	0.03	11.90	−0.001
Global	0.74	0.03	9.86	−0.0003	0.74	0.03	9.86	−0.0003

Schmidt QR-decomposition approach. The MIR statistic was calculated for each metric from a RF model using all non-correlated ALS metrics to determine relative importance for all variables. Next, an iterative subset selection process selected metrics which minimized model mean squared error (MSE) and maximized the percent variation explained. Between four and ten variables were selected for each model (Fig. 2).

While there were no repeat measurements (i.e., pre- and post-fire field observations for the same location) at Pole Creek, there were 48 repeat measurements at Las Conchas. Therefore, additional validation was performed to assess how the PrePost, Pooled, and Global models were able to predict fuel consumption compared to fuel consumption observed as the difference between pre- and post-fire observations. Predicted change was plotted against change observed in 48 plots with repeat measurements and compared using measures of model fit (r-squared, RMSE, RMSE%) and bias (MBE). MBE was calculated as the mean of predicted minus observed values for assessing individual models, but changed to observed minus predicted for assessing change, so that in all reported models negative MBE values would represent underpredicted models and positive MBE would represent model overprediction.

2.3.2. Relationship between biomass consumed and fire radiative energy

The relationship between FRE and biomass consumption can be described as follows:

$$\Delta TF\ [kg] = BCC \times FRE\ [MJ] \tag{4}$$

where ΔTF is the change in total fuel load and BCC is a biomass combustion coefficient derived empirically. Therefore, linear regression was used to characterize the relationship between MODIS-derived estimates of FRE and the sum of all negative ΔTF values within each 1 km MODIS pixel footprint. This analysis was conducted with the hypothesis that the relationship between ΔTF and FRE would be linear and the slope of the regression line (the biomass combustion coefficient: BCC) would be similar to the values proposed in prior studies. FRE was compared only with ΔTF and not the individual fuel load components, since energy observed by MODIS may have originated in any stratum.

Additionally, prior studies have found, and corrected for, a linear bias in FRP and FRE caused by canopy occlusion (Hudak et al., 2016b; Mathews et al., 2016; Roberts et al., 2018). The simple correction proposed by Hudak et al. (2016b) was applied using the formula:

$$FRE_{CC} = FRE_{obs}(1 + COV_{post}) \tag{5}$$

where FRE_{cc} is the canopy cover corrected FRE, FRE_{obs} is the FRE calculated following the methods in Section 2.2.3, and COV_{post} is post-fire canopy cover derived from the percent of first returns above 2 m in the post-fire ALS data. Post-fire canopy cover, rather than pre-fire, was used in the equation because canopy consumption contributed to the observed FRE.

3. Results

3.1. Estimating fuel consumption

RF models were generated for each fuel variable (CF, UF, TF, and CBD) and training data subset (Pre, Post, Pooled, and Global) for both fires. Model performance measures of fit and bias are reported in Table 4. At Las Conchas, the Pre CF model produced the highest r-squared (0.84) and nearly the lowest relative RMSE (9.34%) of any model, while the Post UF model had the lowest r-squared (0.16) and highest relative RMSE (21.4%). At Pole Creek, Global CBD and Pooled TF had the highest r-squared values (both 0.74), but Global CBD had a lower relative RMSE (9.86%). The Post UF model had the lowest r-squared (0.20) and the Pre CBD model had the highest relative RMSE (29.52%).

In terms of temporal generalization, r-squared, RMSE, and MBE for the Pooled models were consistently better than the Post models at Las Conchas, and as good or better than both the Pre and Post models at Pole Creek. To further asses the results of the Pooled models, predicted values were mapped for both fires (Figs. 3 and 4) and areas outside of each fire perimeter were used as a reference conditions to determine if the models were over- or under-predicting fuel changes in relatively unchanged areas. The FACTS database was used to identify and omit 2,427 ha of hazardous fuel reductions outside the Pole Creek fire perimeter that occurred between ALS collections at Pole Creek. After excluding known areas of hazardous fuel reductions, large fuel changes were still observed in the difference between the Pre and Post models (PrePost). Average pixel values for ΔTF outside the Pole Creek fire perimeter were 11.4 (s.d. ± 45.7) Mg ha^{-1} for the PrePost model, −0.1

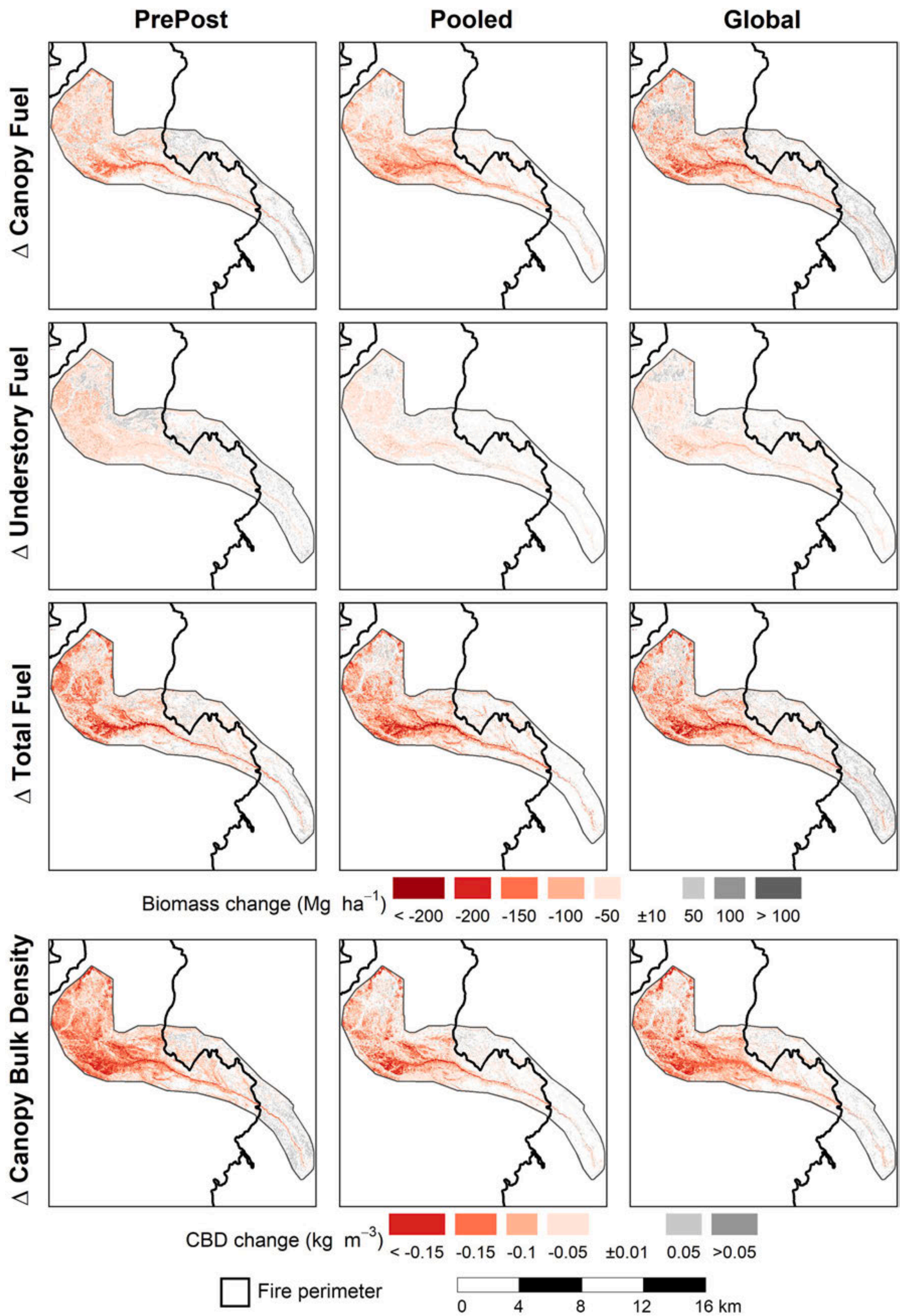

Fig. 3. Mapped estimates of fuel consumption in the Las Conchas, New Mexico, fire using the difference between pre- and post-fire fuel estimates calculated using separate models trained with pre- and post-fire specific field data (PrePost), models trained with the pooled collection of pre- and post-fire field data (Pooled), and models using pooled data from both fires (Global). Along a gradient defined in the legend, red pixels denote fuel consumption, while grey pixels indicate fuel accumulation. (For interpretation of the references to colour in this figure legend, the reader is referred to the web version of this article.)

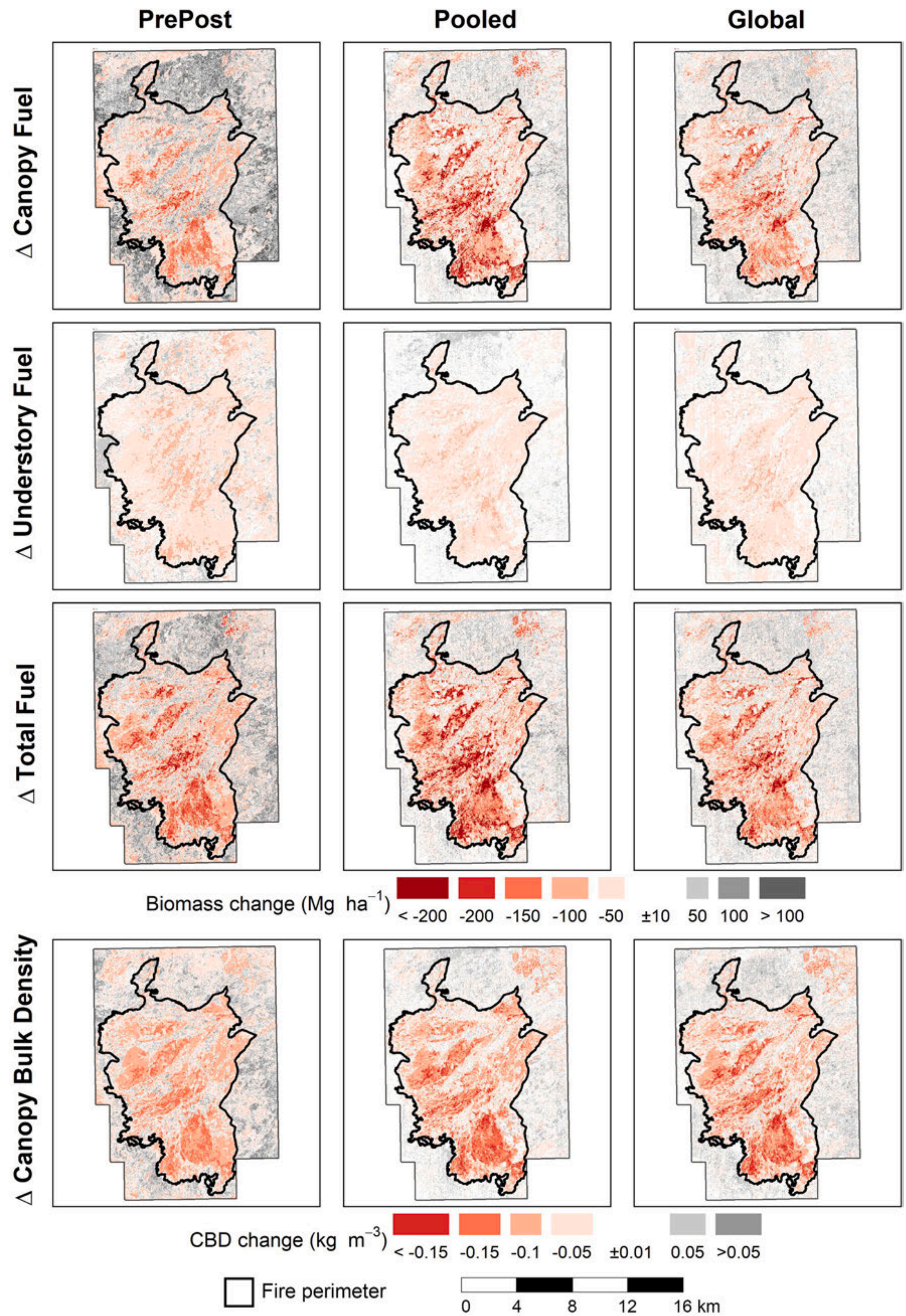

Fig. 4. Mapped estimates of fuel consumption in the Pole Creek, Oregon, fire using the difference between pre- and post-fire fuel estimates calculated using separate models trained with pre- and post-fire specific field data (PrePost), models trained with the pooled collection of pre- and post-fire field data (Pooled), and models using pooled data from both fires (Global). Along a gradient defined in the legend, red pixels denote fuel consumption, while grey pixels indicate fuel accumulation. (For interpretation of the references to colour in this figure legend, the reader is referred to the web version of this article.)

Table 5
Comparison of observed and predicted change at 48 field plots with repeat measurements at the Las Conchas, New Mexico, fire using the difference between pre- and post-fire fuel estimates calculated using separate models trained with pre- and post-fire specific field data (PrePost model), models trained with the pooled collection of pre- and post-fire field data (Pooled model), and models using pooled data from both fires (Global model). Plots comparing field observations and model predictions are displayed in Appendix A, Fig. S3.

	Model performance			
	Las Conchas field plots with repeat measurements			
	r-squared	RMSE	RMSE	MBE
Canopy Fuel		Mg ha^{-1}	%	Mg ha^{-1}
PrePost	0.68	21.80	18.15	−4.62
Pooled	0.65	23.61	19.66	−7.31
Global	0.47	35.95	29.93	−6.29
Understory Fuel		Mg ha^{-1}	%	Mg ha^{-1}
PrePost	0.36	26.10	18.69	3.54
Pooled	0.15	29.10	20.83	−1.77
Global	0.15	29.15	20.87	−0.38
Total Fuel		Mg ha^{-1}	%	Mg ha^{-1}
PrePost	0.67	32.36	17.85	−0.34
Pooled	0.55	38.27	21.11	−8.05
Global	0.40	47.87	26.40	−5.10
Canopy Bulk Density		kg m^3	%	kg m^3
PrePost	0.68	0.05	14.49	−0.01
Pooled	0.68	0.06	16.29	−0.03
Global	0.76	0.05	14.15	−0.02

(s.d. ± 26.7) Mg ha^{-1} for the Pooled model, and 1.2 (s.d. ± 23.9) Mg ha^{-1} for the Global model. The Pre models at Pole Creek also had the smallest number of field observations (n = 9), which resulted in higher relative RMSE (between 21.99% and 29.52%) for all variables, as well as generally lower r-squared values and more bias. Large changes outside the fire perimeter was not observed for the Las Conchas fire, which also had better overall fit and bias in the Pre and Post models. Additionally, no areas of timber harvest or hazardous fuel reductions were observed in the FACTS database between ALS collections. Average pixel values for ΔTF outside the Las Conchas fire perimeter were −4.6 (s.d. ± 19.7) Mg ha^{-1}, −4.9 (s.d. ± 18.8) Mg ha^{-1}, and 0.1 (s.d. ± 19.6) Mg ha^{-1} for the PrePost, Pooled, and Global models.

In assessing spatial generalization, performance of the Pooled and Global models was nominally different, having r-squared values within 0.16 and relative RMSE within 2.04% of each other at both fires. At Las Conchas, the sum of predictions yielded total biomass consumption of 226 Gg for the PrePost model, 224 Gg for the Pooled model, and 224 Gg for the Global model. At Pole Creek, the total biomass consumption was estimated at 581 Gg for the PrePost model, 713 Gg for the Pooled model, and 552 Gg for the Global model.

Repeat measurements for the Las Conchas fire allowed for additional comparison of predicted change versus observed change in 48 of the field plots. Results, shown in Table 5, indicated that the PrePost models had the greatest agreement between predicted and observed values (high r-squared and low RMSE) for ΔCF, ΔUF, and ΔTF, although the Pooled models were not much worse. The Global model had a better fit than the PrePost or Pooled models for estimating ΔCBD but had lower r-squared values and higher RMSE% estimating ΔCF and ΔTF due to a few outliers (Appendix A, Fig. S3).

3.2. Relationship between biomass consumed and fire radiative energy

For both fires, ΔTF estimates using PrePost, Pooled, and Global models were compared with FRE. ΔTF increased linearly with FRE at Las Conchas (Fig. 5) and Pole Creek (Fig. 6). At Las Conchas, the quality

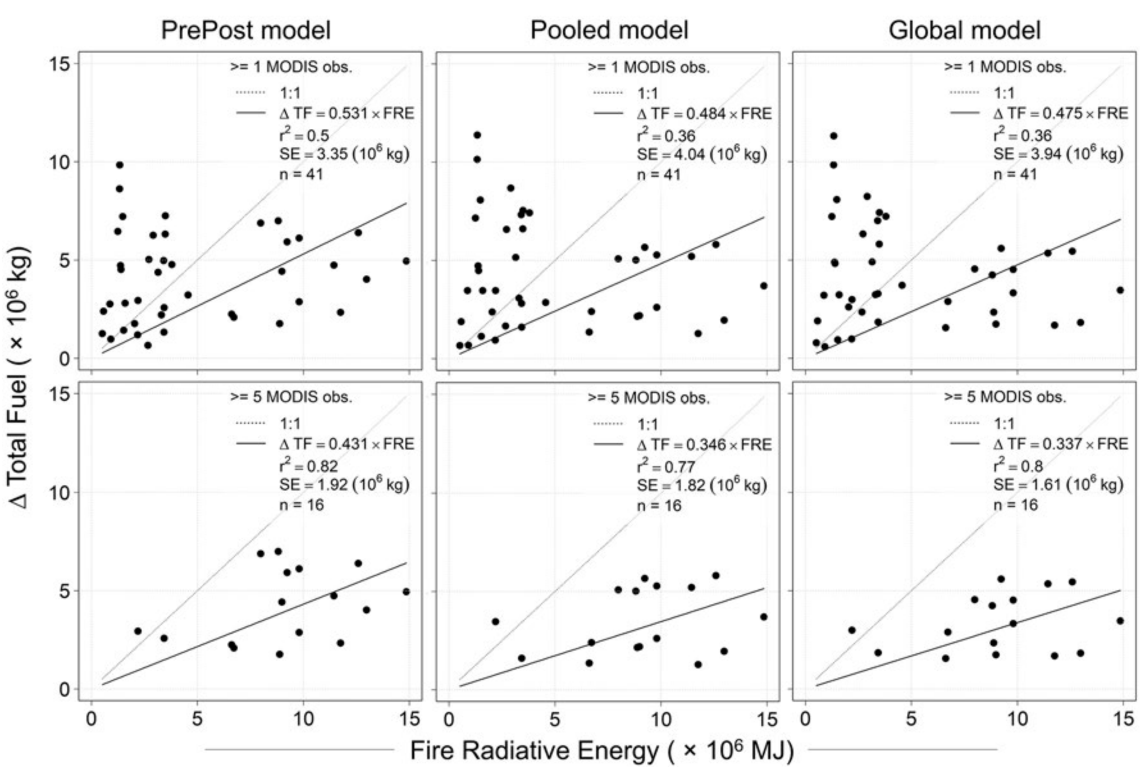

Fig. 5. Fire radiative energy (FRE) compared with change in total fuel (ΔTF) for the Las Conchas, New Mexico, fire using the difference between pre- and post-fire fuel estimates calculated using separate models trained with pre- and post-fire specific field data (PrePost model), models trained with the pooled collection of pre- and post-fire field data (Pooled model), and models using pooled data from both fires (Global model). The rows show how the relationship changes when only pixels with more Moderate Resolution Imaging Spectroradiometer (MODIS) observations are considered. The slope of the line represents the biomass combustion coefficient (BCC; kg MJ^{-1}), which can be used to convert FRE to ΔTF.

of fit between ΔTF and FRE as measured by r-squared and standard error (SE) was better when only pixels with at least five MODIS observations were considered (n = 16) versus using all available MODIS observations (n = 41). At Pole Creek, there was little difference in r-squared and SE values using at least five MODIS observations (n = 109) versus all MODIS observations (n = 147).

Using at least five MODIS observations at Las Conchas, the slope of the regression line, the BCC, was 0.431 kg MJ^{-1} for the PrePost model, 0.346 kg MJ^{-1} for the Pooled model, and 0.337 kg MJ^{-1} for the Global model. The BCC using at least five MODIS observations at Pole Creek was 0.332 kg MJ^{-1} for the PrePost model, 0.428 kg MJ^{-1} Pooled model, and 0.327 kg MJ^{-1} for the Global model. The average BCC for this study (using at least five MODIS observations) was 0.367 (s.d. ± 0.049) kg MJ^{-1}.

4. Discussion

4.1. Estimating fuel consumption

Multitemporal ALS data was demonstrated to be a valuable tool for estimating the consumption of fuel load and density in this study. Additionally, the use of ALS data to quantify fuel has notable advantages over other methods. First, the measurements from ALS can be made at finer-scale than widely used products such as LANDFIRE FCCS (30 m). While this study binned the ALS point cloud at 30 m, high density ALS collections have been used estimate fuel load at resolutions from 5 m (Hudak et al., 2016b) to less than 1 m (Greaves et al., 2016). Second, ALS data incorporates the vertical structure of forest fuels. Optical remote sensing has been used to estimate fuels (Falkowski et al., 2005; Riaño et al., 2002) but doesn't adequately distinguish fuels occluded by canopy layers or differences in vegetation height. A key challenge in measuring fuels across the landscape is high spatial variability of fuel loads across multiple scales (Keane et al., 2013). Therefore, high resolution (horizontal and vertical) ALS-derived fuel consumption maps may have utility for other efforts such as refining fuel classification systems or fire behavior models.

4.1.1. Temporal generalization

One of the most important findings of this study was that pooling pre- and post-fire data yielded comparable or better estimates of fuel consumption to differencing separate pre- and post-fire models. At Las Conchas, where modelled changes from ALS data could be compared to observed changes at 48 permanent field plots, the PrePost models displayed slightly better fit than the Pooled models. However, ΔTF values inside the fire perimeter were near identical, averaging −44.7 (s.d. ± 49.4) Mg ha^{-1} for the PrePost model and − 44.3 (s.d. ± 50.5) Mg ha^{-1} for the Pooled model.

At Pole Creek, large changes in fuel were observed consistently outside the fire perimeter using the PrePost model. Some fuel decrease was expected due to hazardous fuel reduction treatments observed in the FACTS database, such as the CF, TF, and CBD decreases visible outside the fire perimeter in the northeast corner of the ALS data acquisitions (Fig. 4). However, increased CF of over 100 Mg ha^{-1} across large portions of unburned forest was not consistent with any known anthropogenic or natural process over the span of only four years in this ecosystem. This was not an issue for the Las Conchas fire, suggesting that other factors at Pole Creek contributed to the error, such as the small pre-fire sample size and the fact that the post-fire field data captured a wider range of fuel load and density conditions (Table 1). The smaller range of fuel load and density values captured by the pre-fire field plots is notable because it resulted in strong bias for over-predicting biomass at the low end and underpredicting biomass at the high end (Table 4; Appendix A, Fig. S2). Pooling pre- and post-fire plot data corrected the issues outside the fire perimeter, yielded an average ΔTF of −0.1 (s.d. ± 26.7) Mg ha^{-1} compared to 11.4 (s.d. ± 45.7) Mg ha^{-1} using the PrePost model.

The issues with the PrePost model at Pole Creek were not observed in other studies that used separate pre- and post-fire models to quantify change in fuel load (Hudak et al., 2012; Zhao et al., 2018) or fuel density (Skowronski et al., 2014). However, these studies utilized repeat measurements for all or most of their field plots, and both the pre- and post-fire field plots captured a similar range in fuel values. Thus, the data used in these studies were more similar to the data available for the Las Conchas fire, where the PrePost model worked equally well to the Pooled model. These findings demonstrate the importance of capturing a broader range of variation in fuel load and density in the training data for any approach.

Using a single set of training data has practical benefits since pre-fire data collection is a key challenge for fire science due to the inherent uncertainty of where and when wildfires will occur (Lentile et al., 2006; Morgan et al., 2014). In this study, field data that represent a broader range of variation in fuels was a bigger factor than collecting pre-fire field data. Such an approach can be accomplished following a wildfire in most places using a space-for-time sampling scheme, if the full range of fuel load or density can be captured using field data inside and outside the fire perimeter. Additionally, the approach of pooling data across time is supported by other studies. Fekety et al. (2015) found that RF imputation models could accurately predict fuel load across time, and that pooling field data from multiple years improved the models by capturing greater variability in fuel load among the reference observations. Zhao et al. (2018) also demonstrated the ability for models to be trained in one year and applied to another. These studies demonstrated the principle of temporal transferability and generality for ALS-derived biomass models. While this study did not directly test the space-for-time approach, these studies lend confidence to its applicability, especially in fire research where pre-fire field data are scarce. These implications are encouraging for scientists and managers who have multiple ALS data collections without pre-fire field data.

4.1.2. Spatial generalization

Results from Global models using pre- and post-fire data from both fires were encouraging. At Las Conchas, total biomass consumption estimates were highly consistent across all three methods (i.e., PrePost, Pooled, and Global), suggesting both temporal and spatial transferability are technically feasible. In addition to the lack of pre-fire field data, fire scientists and managers are often faced with the absence of any field data. Fekety et al. (2018) demonstrated that models for basal area could be successfully applied in similar ecosystems, thereby providing estimates where field data are scarce or absent. The results of this study suggest that ALS-based models possess even greater generality, as they were tested for two fires 1,600 km apart. However, the transferability of these models was not tested for ecosystems not included in the training data, which may be a topic for future research.

For CBD, the global models consistently outperformed the pooled models in terms of fit and bias for both fires. Additionally, the average predicted decrease in CBD within the fire perimeter was consistent between the pooled and global models for both fires (−0.002 (s.d. ± 0.013) kg m^{-3} versus −0.003 (s.d. ± 0.017) kg m^{-3} for Las Conchas, and − 0.053 (s.d. ± 0.045) kg m^{-3} versus −0.052 (s.d. ± 0.048) kg m^{-3} for Pole Creek). CBD is an indicator of canopy fuel available to burn in a fire and a key measurement for determining whether an active crown fire will spread (Scott and Reinhardt, 2001). Quantification of ΔCBD using a global model across more fires could be used to assess how fire impacts re-burn potential and could provide mechanistic input for modelling crown fire.

Total biomass consumption by the fire derived using the Pooled and Global models was equivalent at Las Conchas (224 Gg vs. 224 Gg) but differed significantly at Pole Creek (713 Gg vs. 552 Gg). Although total biomass consumption estimates for the Global model were similar to PrePost model (581 Gg), there are a few indicators that Global model might be preferable to the Pooled model at Pole Creek. First, the Global model did not exhibit erroneous increases in fuel outside the fire

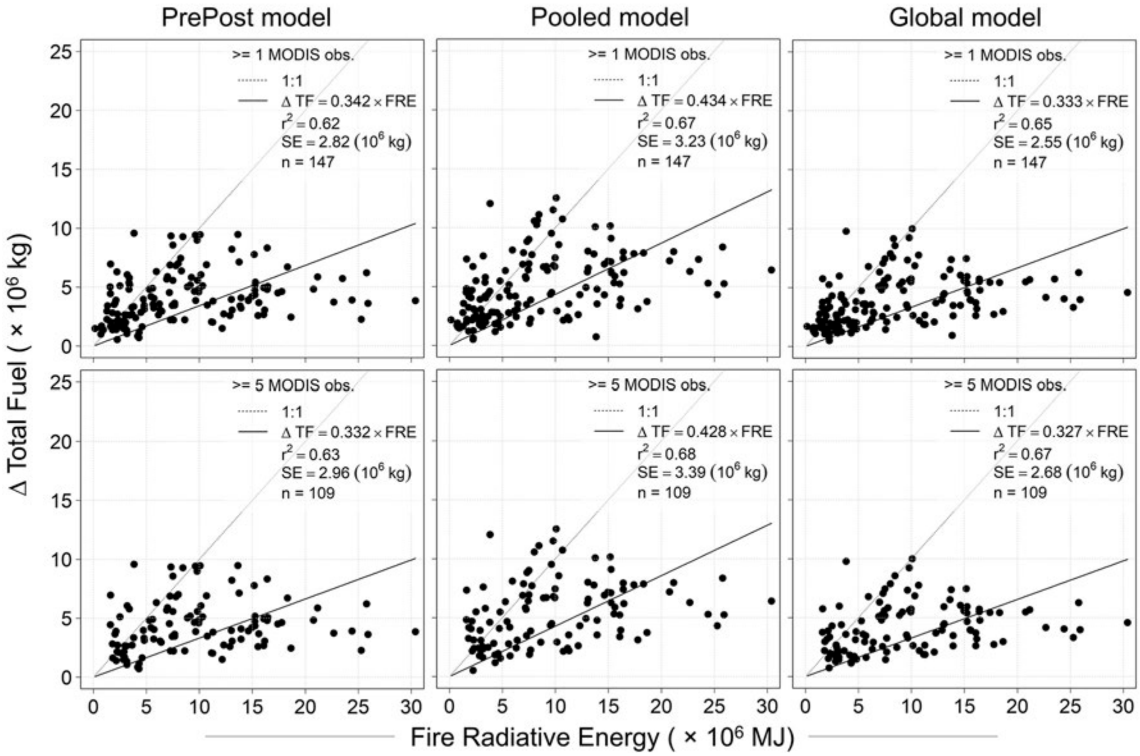

Fig. 6. Fire radiative energy (FRE) compared with change in total fuel (ΔTF) for the Pole Creek, Oregon, fire using the difference between pre- and post-fire fuel estimates calculated using separate models trained with pre- and post-fire specific field data (PrePost model), models trained with the pooled collection of pre- and post-fire field data (Pooled model), and models using pooled data from both fires (Global model). The rows show how the relationship changes when only pixels with more Moderate Resolution Imaging Spectroradiometer (MODIS) observations are considered. The slope of the line represents the biomass combustion coefficient (BCC; kg MJ^{-1}), which can be used to convert FRE to ΔTF.

perimeter like the PrePost model (Fig. 4). Second, while model fit was similar, the Global models exhibited less bias in CF, TF, and CBD than the PrePost or Pooled models (Table 4). This was also true for the Las Conchas fire (Fig. 2). Lastly, comparison with MODIS-derived FRE at Pole Creek (see Section 4.2; Fig. 6) produced lower residual error and a BCC close to estimates by prior studies when using the predictions from the Global model.

4.1.3. Limitations

Models for UF consistently performed worse than CF, TF, or CBD and may prove to be a limitation for applications focused on understory dynamics. However, the results also demonstrated that the models employed in this study have some sensitivity to woody fuels, litter, and duff, which provide little vertical distinction from the ground surface, are often occluded by forest canopies, and are therefore unlikely to be captured directly by ALS measurements. This illustrates the capability of other ALS metrics, including canopy attributes, to indirectly predict otherwise indistinguishable fuels. This idea is supported by other studies that have estimated understory fuel components with ALS data (Bright et al., 2017; Jakubowksi et al., 2013; Pesonen et al., 2008; Price and Gordon, 2016). In fact, the r-squared values for the Pooled and Global UF models in this study (0.34–0.43), were comparable to results from Bright et al. (2017; 0.30) and (Jakubowksi et al., 2013; 0.48), who each observed better model performance by including both optical sensor imagery and ALS metrics in their models. Simultaneous collection of ALS data and optical imagery has been shown elsewhere to more accurately distinguish the true ground surface from low-laying shrubs and herbaceous plants, thereby improving direct measurement of understory vegetation height (Riaño et al., 2007). Future efforts will benefit from increasing availability of platforms that integrate ALS data and optical sensors such as NASA Goddard's Lidar, Hyperspectral and Thermal (G-LiHT) imager (Cook et al., 2013). However, the problem with achieving a well-fitting model also stems from the high spatial variability of fine fuels, which is difficult to capture in the field (Keane and Gray, 2013), and may therefore not improve much unless measured at a finer (sub-meter) scale.

The goal of this study was to capture changes over a relatively short time-period (i.e., the length of the fire), yet data availability reduced certainty that fire was the only process being captured. ALS data were collected one year after the fire in the case of Pole Creek and two years after the fire in the case of Las Conchas. In that time scorched needles and fine branches fall off the trees, thereby changing the fuel profile. Additionally, some tree mortality is delayed, while many shrubs and herbaceous plants begin re-sprouting. Field observations were included if they were within three years of corresponding ALS data, which leaves some uncertainty as to what other ecological processes might have occurred between the field and ALS measurements. These issues were mitigated as best as possible, including comparison with the FACTS database.

In terms of modelling, RF imputation is an alternative method that may improve estimation of UF (Fekety et al., 2015; Hudak et al., 2016a; Hudak et al., 2012). With nearest neighbor RF imputation, CF and UF could be predicted separately while maintaining the complex variance-covariance structure and ensuring that predictions are within the bounds of observations (Eskelson et al., 2009). This method has the distinct advantage of leveraging the connection between the understory and the canopy (Lydersen et al., 2015), where ALS estimation accuracy improves significantly. However, a drawback to this approach was discovered during exploratory analysis in this study. Because the response variable is limited to the values in the observation group, if the full range of variability is not captured or the sample size is too small, then a high degree of change can be observed in relatively unchanged areas when pre- and post-fire fuel estimates are differenced. Essentially this was seen to exacerbate the same problem observed with the PrePost model at Pole Creek. Specific sampling strategies such as oversampling rare structural condition and ensuring large sample size may improve the viability of this approach in future studies as well as being beneficial for the methods employed in this study (Eskelson et al., 2009).

Finally, modelling approaches other than RF deserve consideration. Zhao et al. (2018) found that a linear model had better temporal transferability than RF when measuring forest biomass growth in Scotland. Additionally, a few other studies using multitemporal ALS data have employed a linear model rather than RF (Ma et al., 2018; Meng et al., 2018; Skowronski et al., 2014). Numerous other modelling approaches exist, which provide different advantages depending on the study. Alternatives such as this could be tested to see if they provide better results for spatial generalization of fuel consumption across multiple fires.

4.2. Relationship between biomass consumed and fire radiative energy

The average BCC derived in this study, 0.367 (s.d. ± 0.049) kg MJ^{-1}, was derived under two important conditions. First, the number of MODIS observations was not a major factor at Pole Creek, but the difference across models using at least one MODIS observation and at least five was notable at Las Conchas. This was likely influenced by the greater number of overall observations, as 74% of MODIS pixels had at least five observations at Pole Creek compared to 39% at Las Conchas. The presence of clouds, overpass timing, and fire activity on the ground at the time of overpass are all variables that lead to different number of MODIS observations for different locations within the fire. Therefore, for a given fire multiple observations are not always possible, and the use of single observations are likely to lead to underestimation of biomass consumption.

Second, applying a correction for canopy occlusion as proposed by Hudak et al. (2016b) improved the fit between ΔTF and MODIS-FRE and impacted the final BCCs. Using at least five observations, uncorrected BCCs averaged 0.130 kg MJ^{-1} higher than the corrected values. This effect was slightly more pronounced at Las Conchas, which saw less stand replacing fire than Pole Creek. Multiple studies have noted the impact of forest canopy, demonstrating that estimated consumption of surface fuels decreases linearly with increased canopy occlusion (Mathews et al., 2016; Roberts et al., 2018). The results of this study suggest that canopy occlusion is an important factor to consider for future MODIS-based estimated of biomass consumption.

The BCC values of this study (0.367 (s.d. ± 0.049) kg MJ^{-1}) are highly consistent with values proposed by others. The most similar study in terms of scale of analysis (i.e., multiple fires) is Li et al. (2018), which arrived at a slightly lower value of 0.301 kg MJ^{-1} using MODIS FRE across 445 fires. Several laboratory experiments, such as (Wooster et al., 2005; 0.368 kg MJ^{-1}) and (Smith et al., 2013; 0.325 kg MJ^{-1}), are very close to the BCC derived here. The average BCC in the study is below laboratory-derived estimates from (Freeborn et al., 2008; 0.453 kg MJ^{-1}) and higher than the field-based experiment conducted by (Kremens et al., 2012; 0.2986 kg MJ^{-1}).

Wooster (2002) and Wooster et al. (2005) suggested that FRE is linearly related to biomass consumption regardless of fuel geometry and vegetation type. This idea is corroborated by the fact that similar BCCs were derived at both fires in this study, despite the fires occurring in different ecosystems. Confirming a consistent BCC at multiple scales has broad implications for estimating regional and global biomass consumption and, in turn, carbon emission estimates. It suggests that MODIS FRE provides a valuable alternative to the burned area approach presented by Seiler and Crutzen (1980), as it does not require pre-fire fuel load or combustion completeness. However, sufficient MODIS observations and accounting of canopy occlusion should be considered. Future work to accurately estimate carbon emissions from fires globally will likely rely on a suite of products, which include burned area estimates, FRE retrieval, and models for fuel load consumption.

5. Conclusion

This study explores a relatively new method for estimating landscape-scale fuel consumption by using multitemporal airborne laser scanning (ALS) data calibrated with pre- and post-fire field data. Most importantly, the analysis demonstrated that capturing a broad range of fuel conditions in the training data is more important than having separate pre- and post-fire models. Due to the unpredictable nature of wildfire, pre-fire field observations are typically rare. Therefore, these results are noteworthy for scientists and managers who have pre- and post-fire ALS data collections and wish to use a space-for-time approach to capture pre-fire fuel load or fuel density. This study also found that models could be generalized to estimate fuel consumption between two forested ecosystems in the western U.S. and that, like pooling pre- and post-fire field data, using data from multiple fires yielded comparable results. Analysis confirmed the linearity of the relationship between change in total fuel load (ΔTF) and fire radiative energy (FRE) and the resulting biomass combustion coeifficients (BCCs) were comparable to those derived in laboratory and small field-based experiments. Additionally, this study found that accounting for canopy occlusion and using areas with multiple Moderate Resolution Imaging Spectroradiometer (MODIS)-FRE observations were both important factors. These results highlight considerations that should be made when estimating biomass consumption from MODIS-FRE and support prior work synthesizing a consistent BCC at multiple scales.

Declaration of Competing Interest

None.

Acknowledgements

The authors are grateful for valuable feedback from internal and external reviewers. This work was supported by Joint Fire Sciences Program projects 15-S-01-01 and 16-4-01-15, NASA project 17-FIRECHM17-0036, and the USFS Rocky Mountain Research Station under Joint Venture Agreements 17-JV-11221633-166 and 19-JV-11221633-165 with the University of Idaho. This manuscript is submitted for publication with the understanding that the United States Government is authorized to reproduce and distribute reprints for governmental purposes. Any use of trade, product, or firm names is for descriptive purposes only and does not imply endorsement by the United States Government.

Appendix A. Supplementary data

Supplementary data to this article can be found online at https://doi.org/10.1016/j.rse.2020.112114.

References

Abatzoglou, J.T., Williams, A.P., 2016. Impact of anthropogenic climate change on wildfire across Western US forests. Proc. Natl. Acad. Sci. 201607171https://doi.org/10.1073/pnas.1607171113. In press.

Alonzo, M., Morton, D.C., Cook, B.D., Andersen, H.-E., Babcock, C., Pattison, R., 2017. Patterns of canopy and surface layer consumption in a boreal forest fire from repeat airborne lidar. Environ. Res. Lett. 12, 065004. https://doi.org/10.1088/1748-9326/aa6ade.

Andersen, H.-E., McGaughey, R.J., Reutebuch, S.E., 2005. Estimating forest canopy fuel parameters using LIDAR data. Remote Sens. Environ. 94, 441–449. https://doi.org/10.1016/j.rse.2004.10.013.

Andreae, M.O., Merlet, P., 2001. Emission of trace gases and aerosols from biomass burning. Glob. Biogeochem. Cycles 15, 955–966.

Boschetti, L., Roy, D.P., 2009. Strategies for the fusion of satellite fire radiative power with burned area data for fire radiative energy derivation. J. Geophys. Res. 114. https://doi.org/10.1029/2008JD011645.

Bowman, D.M.J.S., Balch, J.K., Artaxo, P., Bond, W.J., Carlson, J.M., Cochrane, M.A., Antonio, C.M.D., Defries, R.S., Doyle, J.C., Harrison, S.P., Johnston, F.H., Keeley, J.E., Krawchuk, M.A., Kull, C.A., Marston, J.B., Moritz, M.A., Prentice, I.C., Roos, C.I., Scott, A.C., Swetnam, T.W., Van Der Werf, G.R., Pyne, S.J., 2009. Fire in the earth

system. Science 324, 481–484. https://doi.org/10.1126/science.1163886.
Breiman, L., 2001. Random forests. Mach. Learn. 45, 5–32.
Bright, B., Hudak, A., Meddens, A., Hawbaker, T., Briggs, J., Kennedy, R., 2017. Prediction of forest canopy and surface fuels from Lidar and satellite time series data in a bark beetle-affected forest. Forests 8, 322. https://doi.org/10.3390/f8090322.
Brown, J.K., Oberhau, R.D., Johnston, C.M., 1982. Handbook for Inventorying Surface Fuels and Biomass in the Interior West, General Technical Report INT-129. USDA Forest Service, Intermountain Forest and Range Experiment Station, Ogden, UT.
Chasmer, L.E., Hopkinson, C.D., Petrone, R.M., Sitar, M., 2017. Using multitemporal and multispectral airborne Lidar to assess depth of peat loss and correspondence with a new active normalized burn ratio for wildfires. Geophys. Res. Lett. 44, 11,851–11,859. https://doi.org/10.1002/2017GL075488.
Chuvieco, E., Mouillot, F., van der Werf, G.R., San Miguel, J., Tanase, M., Koutsias, N., García, M., Yebra, M., Padilla, M., Gitas, I., Heil, A., Hawbaker, T.J., Giglio, L., 2019. Historical background and current developments for mapping burned area from satellite earth observation. Remote Sens. Environ. 225, 45–64. https://doi.org/10.1016/j.rse.2019.02.013.
Cook, B.D., Corp, L.A., Nelson, R.F., Middleton, E.M., Morton, D.C., McCorkel, J.T., Masek, J.G., Ranson, K.J., Ly, V., Montesano, P.M., 2013. NASA goddard's LiDAR, hyperspectral and thermal (G-LiHT) airborne imager. Remote Sens. 5, 4045–4066. https://doi.org/10.3390/rs5084045.
Eidenshink, J., Schwind, B., Brewer, K., Zhu, Z., Quayle, B., Howard, S., 2007. A project for monitoring trends in burn severity. Fire Ecol. Spec. Issue 3, 3–21.
Eskelson, B.N.I., Temesgen, H., Lemay, V., Barrett, T.M., Crookston, N.L., Hudak, A.T., 2009. The roles of nearest neighbor methods in imputing missing data in forest inventory and monitoring databases. Scand. J. For. Res. 24, 235–246. https://doi.org/10.1080/02827580902870490.
Evans, J.S., Murphy, M.A., 2017. rfUtilities: Random Forests Model Selection and Performace Evaluation. [WWW document]. R Packag Version 2.1-1. URL. http://cran.r-project.org/package=rfUtilities.
Falkowski, M.J., Gessler, P.E., Morgan, P., Hudak, A.T., Smith, A.M.S., 2005. Characterizing and mapping forest fire fuels using ASTER imagery and gradient modeling. For. Ecol. Manag. 217, 129–146. https://doi.org/10.1016/j.foreco.2005.06.013.
Fekety, P.A., Falkowski, M.J., Hudak, A.T., 2015. Temporal transferability of LiDAR-based imputation of forest inventory attributes. Can. J. For. Res. 45, 422–435. https://doi.org/10.1139/cjfr-2014-0405.
Fekety, P.A., Falkowski, M.J., Hudak, A.T., Jain, T.B., Evans, J.S., 2018. Transferability of Lidar-derived basal area and stem density models within a northern Idaho ecoregion. Can. J. Remote. Sens. 44, 131–143. https://doi.org/10.1080/07038992.2018.1461557.
Freeborn, P.H., Wooster, M.J., Hao, W.M., Ryan, C.A., Nordgren, B.L., Baker, S.P., Ichoku, C., 2008. Relationships between energy release, fuel mass loss, and trace gas an aerosol emissions during laboratory biomass fires. J. Geophys. Res. Atmos. 113, 1–17. https://doi.org/10.1029/2007JD008679.
Freeborn, P.H., Wooster, M.J., Roberts, G., 2011. Addressing the spatiotemporal sampling design of MODIS to provide estimates of the fire radiative energy emitted from Africa. Remote Sens. Environ. 115, 475–489. https://doi.org/10.1016/j.rse.2010.09.017.
French, N.H.F., De Groot, W.J., Jenkins, L.K., Rogers, B.M., Alvarado, E., Amiro, B., De Jong, B., Goetz, S., Hoy, E., Hyer, E., Keane, R., Law, B.E., McKenzie, D., McNulty, S.G., Ottmar, R., Pérez-Salicrup, D.R., Randerson, J., Robertson, K.M., Turetsky, M., 2011. Model comparisons for estimating carbon emissions from north American wildland fire. J. Geophys. Res. Biogeosci. 116. https://doi.org/10.1029/2010JG001469.
García, M., Saatchi, S., Casas, A., Koltunov, A., Ustin, S., Ramirez, C., Garcia-Gutierrez, J., Balzter, H., 2017. Quantifying biomass consumption and carbon release from the California rim fire by integrating airborne LiDAR and Landsat OLI data. J. Geophys. Res. Biogeosci. 122, 340–353. https://doi.org/10.1002/2015JG003315.
Giglio, L., Schroeder, W., Justice, C.O., 2016. The collection 6 MODIS active fire detection algorithm and fire products. Remote Sens. Environ. 178, 31–41. https://doi.org/10.1016/j.rse.2016.02.054.
Giglio, L., Boschetti, L., Roy, D.P., Humber, M.L., Justice, C.O., 2018. The collection 6 MODIS burned area mapping algorithm and product. Remote Sens. Environ. 217, 72–85. https://doi.org/10.1016/j.rse.2018.08.005.
Gillespie, A.J.R., 1999. Rationale for a National Annual Forest Inventory Program. J. For. 97, 16–20.
González-Ferreiro, E., Diéguez-Aranda, U., Crecente-Campo, F., Barreiro-Fernández, L., Miranda, D., Castedo-Dorado, F., 2014. Modelling canopy fuel variables for *Pinus radiata* D. Don in NW Spain with low-density LiDAR data. Int. J. Wildland Fire 23, 350. https://doi.org/10.1071/WF13054.
Greaves, H.E., Vierling, L.A., Eitel, J.U.H., Boelman, N.T., Magney, T.S., Prager, C.M., Griffin, K.L., 2016. High-resolution mapping of aboveground shrub biomass in Arctic tundra using airborne lidar and imagery. Remote Sens. Environ. 184, 361–373. https://doi.org/10.1016/j.rse.2016.07.026.
Hoe, M.S., Dunn, C.J., Temesgen, H., 2018. Multitemporal LiDAR improves estimates of fire severity in forested landscapes. Int. J. Wildland Fire 27, 581. https://doi.org/10.1071/WF17141.
Hu, T., Ma, Q., Su, Y., Battles, J.J., Collins, B.M., Stephens, S.L., Kelly, M., Guo, Q., 2019. A simple and integrated approach for fire severity assessment using bi-temporal airborne LiDAR data. Int. J. Appl. Earth Obs. Geoinf. 78, 25–38. https://doi.org/10.1016/j.jag.2019.01.007.
Hudak, A.T., Strand, E.K., Vierling, L.A., Byrne, J.C., Eitel, J.U.H., Martinuzzi, S., Falkowski, M.J., 2012. Quantifying aboveground forest carbon pools and fluxes from repeat LiDAR surveys. Remote Sens. Environ. 123, 25–40. https://doi.org/10.1016/j.rse.2012.02.023.
Hudak, A.T., Bright, B.C., Pokswinski, S.M., Loudermilk, E.L., O'Brien, J.J., Hornsby, B.S., Klauberg, C., Silva, C.A., 2016a. Mapping Forest structure and composition from low-density LiDAR for informed Forest, fuel, and fire management at Eglin air force base, Florida, USA. Can. J. Remote. Sens. 42, 411–427. https://doi.org/10.1080/07038992.2016.1217482.
Hudak, A.T., Dickinson, M.B., Bright, B.C., Kremens, R.L., Loudermilk, E.L., O'Brien, J.J., Hornsby, B.S., Ottmar, R.D., 2016b. Measurements relating fire radiative energy density and surface fuel consumption–RxCADRE 2011 and 2012. Int. J. Wildland Fire 25, 25–37. https://doi.org/10.1071/WF14159.
Isenburg, M., 2013. LAStools - Efficient Tools for LiDAR Processing. [WWW Document] URL. http://lastools.org.
Jakubowksi, M.K., Guo, Q., Collins, B., Stephens, S., Kelly, M., 2013. Predicting Surface Fuel Models and Fuel Metrics Using Lidar. 79. pp. 37–49.
Kaufman, Y.J., Remer, L., Ottmar, R., Ward, D., Rong-R, L., Kleidman, R., Fraser, R., Flynn, L., McDougal, D., Shelton, G., 1996. Relationships between remotely sensed fire intensity and rate of emission of smoke: SCAR-C experiment. In: Levine, J. (Ed.), Global Biomass Burning. MIT Press, Massachusetts, pp. 685–696.
Keane, R.E., Gray, K., 2013. Comparing three sampling techniques for estimating fine woody down dead biomass. Int. J. Wildland Fire 22, 1093–1107. https://doi.org/10.1071/WF13038.
Keane, R.E., Herynk, J.M., Toney, C., Urbanski, S.P., Lutes, D.C., Ottmar, R.D., 2013. Evaluating the performance and mapping of three fuel classification systems using Forest inventory and analysis surface fuel measurements. For. Ecol. Manag. 305, 248–263. https://doi.org/10.1016/j.foreco.2013.06.001.
Klauberg, C., Hudak, A.T., Bright, B.C., Boschetti, L., Dickinson, M.B., Kremens, R.L., Silva, C.A., 2018. Use of ordinary kriging and Gaussian conditional simulation to interpolate airborne fire radiative energy density estimates. Int. J. Wildland Fire 27, 228–240. https://doi.org/10.1071/WF17113.
Kolden, C.A., Smith, A.M.S., Abatzoglou, J.T., 2015. Limitations and utilisation of monitoring trends in burn severity products for assessing wildfire severity in the USA. Int. J. Wildland Fire 24. https://doi.org/10.1071/WF15082.
Kremens, R.L., Dickinson, M.B., Bova, A.S., 2012. Radiant flux density, energy density and fuel consumption in mixed-oak forest surface fires. Int. J. Wildland Fire 21, 722–730. https://doi.org/10.1071/WF10143.
Lentile, L.B., Holden, Z.A., Smith, A.M.S., Falkowski, M.J., Hudak, A.T., Morgan, P., Lewis, S.A., Gessler, P.E., Benson, N.C., 2006. Remote sensing techniques to assess active fire characteristics and post-fire effects. Int. J. Wildland Fire 15, 319–345. https://doi.org/10.1071/WF05097.
Li, F., Zhang, X., Kondragunta, S., Roy, D.P., 2018. Investigation of the fire Radiative energy biomass combustion coefficient: a comparison of polar and geostationary satellite retrievals over the conterminous United States. J. Geophys. Res. Biogeosci. 123, 722–739. https://doi.org/10.1002/2017JG004279.
Lydersen, J.M., Collins, B.M., Knapp, E.E., Roller, G.B., Stephens, S., 2015. Relating fuel loads to overstorey structure and composition in a fire-excluded Sierra Nevada mixed conifer forest. Int. J. Wildland Fire 24, 484–494. https://doi.org/10.1071/WF13066.
Ma, Q., Su, Y., Luo, L., Li, L., Kelly, M., Guo, Q., 2018. Evaluating the uncertainty of Landsat-derived vegetation indices in quantifying forest fuel treatments using bi-temporal LiDAR data. Ecol. Indic. 95, 298–310. https://doi.org/10.1016/j.ecolind.2018.07.050.
Mathews, B.J., Strand, E.K., Smith, A.M.S., Hudak, A.T., Dickinson, B., Kremens, R.L., 2016. Laboratory experiments to estimate interception of infrared radiation by tree canopies. Int. J. Wildland Fire 25, 1009–1014. https://doi.org/10.1071/WF16007.
McCarley, T.R., Kolden, C.A., Vaillant, N.M., Hudak, A.T., Smith, A.M.S., Wing, B.M., Kellogg, B.S., Kreitler, J., 2017. Multi-temporal LiDAR and Landsat quantification of fire-induced changes to forest structure. Remote Sens. Environ. 191, 419–432. https://doi.org/10.1016/j.rse.2016.12.022.
McCarley, T.R., Smith, A.M.S., Kolden, C.A., Kreitler, J., 2018. Evaluating the mid-infrared bi-spectral index for improved assessment of low-severity fire effects in a conifer forest. Int. J. Wildland Fire 27, 407. https://doi.org/10.1071/WF17137.
McGaughey, R.J., 2014. FUSION/LDV: Software for LIDAR Data Analysis and Visualization. USDA Forest Service, Pacific Northwest Research Station.
McKenzie, D., Raymond, C.L., Kellogg, L.-K.B., Norheim, R.A., Andreu, A.G., Bayard, A.C., Kopper, K.E., Elman, E., 2007. Mapping fuels at multiple scales: landscape application of the fuel characteristic classification system. Can. J. For. Res. 37, 2421–2437. https://doi.org/10.1139/X07-056.
Meng, R., Dennison, P.E., Zhao, F., Shendryk, I., Rickert, A., Hanavan, R.P., Cook, B.D., Serbin, S.P., 2018. Mapping canopy defoliation by herbivorous insects at the individual tree level using bi-temporal airborne imaging spectroscopy and LiDAR measurements. Remote Sens. Environ. 215, 170–183. https://doi.org/10.1016/j.rse.2018.06.008.
Morgan, P., Keane, R.E., Dillon, G.K., Jain, T.B., Hudak, A.T., Karau, E.C., Sikkink, P.G., Holden, Z.A., Strand, E.K., 2014. Challenges of assessing fire and burn severity using field measures, remote sensing and modelling. Int. J. Wildland Fire 23, 1045. https://doi.org/10.1071/WF13058.
Murphy, M.A., Evans, J.S., Storfer, A., 2010. Quantifying *Bufo boreas* connectivity in Yellowstone National Park with landscape genetics. Ecology 91, 252–261. https://doi.org/10.1890/08-0879.1.
Ottmar, R.D., 2014. Wildland fire emissions, carbon, and climate: modeling fuel consumption. For. Ecol. Manag. 317, 41–50. https://doi.org/10.1016/j.foreco.2013.06.010.
Ottmar, R.D., Sandberg, D.V., Riccardi, C.L., Prichard, S.J., 2007. An overview of the fuel characteristic classification system — quantifying, classifying, and creating fuelbeds for resource planning. Can. J. For. Res. 37, 2383–2393. https://doi.org/10.1139/X07-077.
Pesonen, A., Maltamo, M., Eerikäinen, K., Packalèn, P., 2008. Airborne laser scanning-based prediction of coarse woody debris volumes in a conservation area. For. Ecol. Manag. 255, 3288–3296. https://doi.org/10.1016/j.foreco.2008.02.017.

Price, O.F., Gordon, C.E., 2016. The potential for LiDAR technology to map fire fuel hazard over large areas of Australian forest. J. Environ. Manag. 181, 663–673. https://doi.org/10.1016/j.jenvman.2016.08.042.
Prichard, S.J., Larkin, N., Ottmar, R., French, N., Baker, K., Brown, T., Clements, C., Dickinson, M., Hudak, A., Kochanski, A., Linn, R., Liu, Y., Potter, B., Mell, W., Tanzer, D., Urbanski, S., Watts, A., 2019. The fire and smoke model evaluation experiment—a plan for integrated, large fire–atmosphere field campaigns. Atmosphere (Basel) 10, 66. https://doi.org/10.3390/atmos10020066.
Randerson, J.T., Chen, Y., van der Werf, G.R., Rogers, B.M., Morton, D.C., 2012. Global burned area and biomass burning emissions from small fires. J. Geophys. Res. Biogeosci. 117. https://doi.org/10.1029/2012JG002128.
Reinhardt, E.D., Crookston, N.L., 2003. Fire and Fuels Extension to the Forest Vegetation Simulator. USDA Forest Service, General Technical Report RMRS-GTR-116.
Riaño, D., Chuvieco, E., Salas, J., Palacios-Orueta, A., Bastarrika, A., 2002. Generation of fuel type maps from Landsat TM images and ancillary data in Mediterranean ecosystems. Can. J. For. Res. 32, 1301–1315. https://doi.org/10.1139/x02-052.
Riaño, D., Meier, E., Allgower, B., 2003. Modeling airborne laser scanning data for the spatial generation of critical forest parameters in fire behavior modeling. Remote Sens. Environ. 86, 177–186. https://doi.org/10.1016/S0034-4257(03)00098-1.
Riaño, D., Chuvieco, E., Condés, S., González-Matesanz, J., Ustin, S.L., 2004. Generation of crown bulk density for *Pinus sylvestris* L. from lidar. remote sens. Environ. 92, 345–352. https://doi.org/10.1016/j.rse.2003.12.014.
Riaño, D., Chuvieco, E., Ustin, S.L., Salas, J., Rodríguez-Pérez, J.R., Ribeiro, L.M., Viegas, D.X., Moreno, J.M., Fernández, H., 2007. Estimation of shrub height for fuel-type mapping combining airborne LiDAR and simultaneous color infrared ortho imaging. Int. J. Wildland Fire 16, 341–348. https://doi.org/10.1071/WF06003.
Roberts, G., Wooster, M.J., Lauret, N., Gastellu-Etchegorry, J.P., Lynham, T., McRae, D., 2018. Investigating the impact of overlying vegetation canopy structures on fire radiative power (FRP) retrieval through simulation and measurement. Remote Sens. Environ. 217, 158–171. https://doi.org/10.1016/j.rse.2018.08.015.
Roteta, E., Bastarrika, A., Padilla, M., Storm, T., Chuvieco, E., 2019. Development of a sentinel-2 burned area algorithm: generation of a small fire database for sub-Saharan Africa. Remote Sens. Environ. 222, 1–17. https://doi.org/10.1016/j.rse.2018.12.011.
Roussel, J.-R., Auty, D., 2019. lidR: Airborne LiDAR Data Manipulation and Visualization for Forestry Applications. [WWW document]. R Packag Version 2.1.3. URL. https://cran.r-project.org/package=lidR.
Roy, D.P., Landmann, T., 2005. Characterizing the surface heterogeneity of fire effects using multi-temporal reflective wavelength data. Int. J. Remote Sens. 26, 4197–4218. https://doi.org/10.1080/01431160500112783.
Roy, D.P., Huang, H., Boschetti, L., Giglio, L., Yan, L., Zhang, H.H., Li, Z., 2019. Landsat-8 and Sentinel-2 burned area mapping – a combined sensor multi-temporal change detection approach. Remote Sens. Environ. 231, 111254. https://doi.org/10.1016/j.rse.2019.111254.
Scott, J.H., Reinhardt, E.D., 2001. Assessing crown fire potential by linking models of surface and crown fire behavior. In: Research Paper RMRS-RP-29. U.S. Department of Agriculture, Forest Service, Rocky Mountain Research Station. https://doi.org/10.2737/RMRS-RP-29.
Seiler, W., Crutzen, P.J., 1980. Estimates of gross and net fluxes of carbon between the biosphere and the atmosphere from biomass burning. Clim. Chang. 2, 207–247. https://doi.org/10.1007/BF00137988.
Skowronski, N.S., Clark, K.L., Gallagher, M., Birdsey, R.A., Hom, J.L., 2014. Airborne laser scanner-assisted estimation of aboveground biomass change in a temperate oak-pine forest. Remote Sens. Environ. 151, 166–174. https://doi.org/10.1016/j.rse.2013.12.015.
Smith, A.M.S., Wooster, M.J., Drake, N.A., Dipotso, F.M., Perry, G.L.W., 2005. Fire in African savanna: testing the impact of incomplete combustion on pyrogenic emissions estimates. Ecol. Appl. 15, 1074–1082. https://doi.org/10.1890/03-5256.
Smith, A.M.S., Tinkham, W.T., Roy, D.P., Boschetti, L., Kremens, R.L., Kumar, S.S., Sparks, A.M., Falkowski, M.J., 2013. Quantification of fuel moisture effects on biomass consumed derived from fire radiative energy retrievals. Geophys. Res. Lett. 40, 6298–6302. https://doi.org/10.1002/2013GL058232.
Sparks, A.M., Boschetti, L., Smith, A.M.S., Tinkham, W.T., Lannom, K.O., Newingham, B.A., 2015. An accuracy assessment of the MTBS burned area product for shrub-–steppe fires in the northern Great Basin, United States. Int. J. Wildland Fire 24, 70. https://doi.org/10.1071/WF14131.
USDA Forest Service, 2015. Forest Activity Tracking System. [WWW Document]. URL. http://data.fs.usda.gov/geodata/edw/datasets.php (accessed 12.9.15).
Van Der Werf, G.R., Randerson, J.T., Collatz, G.J., Giglio, L., Kasibhatla, P.S., Arellano, A.F., Olsen, S.C., Kasischke, E.S., 2004. Continental-scale partitioning of fire emissions during the 1997 to 2001 El Niño/La Niña period. Science 303, 73–76. https://doi.org/10.1126/science.1090753.
Van Der Werf, G.R., Randerson, J.T., Giglio, L., Collatz, G.J., Mu, M., Kasibhatla, P.S., Morton, D.C., Defries, R.S., Jin, Y., Van Leeuwen, T.T., 2010. Global fire emissions and the contribution of deforestation, savanna, forest, agricultural, and peat fires (1997–2009). Atmos. Chem. Phys. 10, 11707–11735. https://doi.org/10.5194/acp-10-11707-2010.
Van Der Werf, G.R., Randerson, J.T., Giglio, L., Van Leeuwen, T.T., Chen, Y., Rogers, B.M., Mu, M., Van Marle, M.J.E., Morton, D.C., Collatz, G.J., Yokelson, R.J., Kasibhatla, P.S., 2017. Global fire emissions estimates during 1997–2016. Earth Syst. Sci. Data 9, 697–720. https://doi.org/10.5194/essd-9-697-2017.
Westerling, A.L., Hidalgo, H.G., Cayan, D.R., Swetnam, T.W., 2006. Warming and earlier spring increase Western U.S. Forest wildfire activity. Science 313, 940–943. https://doi.org/10.1126/science.1128834.
Wooster, M.J., 2002. Small-scale experimental testing of fire radiative energy for quantifying mass combusted in natural vegetation fires. Geophys. Res. Lett. 29, 21–24. https://doi.org/10.1029/2002GL015487.
Wooster, M.J., Roberts, G., Perry, G.L.W., Kaufman, Y.J., 2005. Retrieval of biomass combustion rates and totals from fire radiative power observations: FRP derivation and calibration relationships between biomass consumption and fire radiative energy release. J. Geophys. Res. 110, D24311. https://doi.org/10.1029/2005JD006318.
Wulder, M.A., White, J.C., Alvarez, F., Han, T., Rogan, J., Hawkes, B., 2009. Characterizing boreal forest wildfire with multi-temporal Landsat and LIDAR data. Remote Sens. Environ. 113, 1540–1555. https://doi.org/10.1016/j.rse.2009.03.004.
Zhao, K., Suarez, J.C., Garcia, M., Hu, T., Wang, C., Londo, A., 2018. Utility of multitemporal lidar for forest and carbon monitoring: tree growth, biomass dynamics, and carbon flux. Remote Sens. Environ. 204, 883–897. https://doi.org/10.1016/j.rse.2017.09.007.